


 CrossMark
click for updates

Cite this: DOI: 10.1039/c6lc00534a

A simple acoustofluidic chip for microscale manipulation using evanescent Scholte waves†

 Vivian Aubert,^{ab} Régis Wunenburger,^c Tony Valier-Brasier,^c David Rabaud,^{ab} Jean-Philippe Kleman^{def} and Cédric Poulain^{*ab}

Acoustofluidics is acknowledged as a powerful tool offering a contactless and label-free manipulation of fluids, micro-beads, and living cells. To date, most techniques rely on the use of propagating acoustic waves and take advantage of the associated acoustic radiation force in standing or progressive fields. Here, we present a new approach based on the generation of an evanescent acoustic field above a substrate. This field is obtained by means of subsonic interfacial waves giving rise to a well-defined standing wave pattern. By both imaging and probing the evanescent acoustic field, we show that these interfacial waves are guided waves known as quasi-Scholte acoustic waves. Scholte waves present very interesting features for applications in acoustofluidics. Namely, they confine the acoustic energy to the vicinity of the surface, they are nearly lossless and thus can propagate over long distances along the substrate, and finally they do not require any particular material for the substrate. With a very simple and low-cost device we show several examples of applications including patterning lines or arrays of cells, triggering spinning of living cells, and separating plasma from RBC in a whole blood microdroplet.

 Received 22nd April 2016,
Accepted 1st June 2016

DOI: 10.1039/c6lc00534a

www.rsc.org/loc

Introduction

Acoustic manipulation of fluids and particles at both micro or nano-scale has become a very active field of research in the last decade.^{1,2} It has been shown that the use of acoustic waves enables nanoparticles,³ micro-bubbles,^{4,5} drops or microbeads, living cells⁶ and fluids to be moved, sorted, or mixed in a contactless and label-free manner, depending on their relative density, compressibility or size. Most of the applications and their associated techniques rely on the acoustic radiation force and acoustic streaming effect which are both of non linear origin and whose amplitude scales with the gradient of the pressure field. Thus, small acoustic wavelengths are in general favourable to maximise both effects. Hence, both high frequencies and high acoustic pressure are usually required in order to increase the spatial energy gradients.

In practice, acoustic generation is achieved using mostly two techniques: BAW-based (bulk acoustic wave) and SAW-

based (surface acoustic wave) devices^{1,7} with acoustic amplitude typically in the 0.1–1 MPa range.^{8,9} Whereas BAW are bulk longitudinal acoustic waves propagating within the bulk of the liquid, SAW are surface acoustic waves propagating along the substrate surface. Usually, in a BAW-based microfluidic device the liquid volume is used as a resonant cavity. Thus, the device has to be made of materials offering a high acoustic impedance mismatch with the liquid, classically silicon or glass. Moreover, it is designed to operate at a specific frequency (lying in the MHz range) such that the channel width matches a multiple of half-wavelength of the longitudinal standing wave formed.¹⁰ In most cases, SAW devices are based on the use of Rayleigh waves⁹ and less frequently on Lamb waves^{11,12} propagating along a substrate and radiating into the fluid bulk. Typically, high frequency have to be used to ensure a wavelength much smaller than the substrate thickness d , as required for Rayleigh wave excitation as well as to increase the radiation pressure. This working frequency f is determined by the pitch of the IDT (interdigitated transducer) deposited onto the piezoelectric substrate designed for actuation and is classically around 40 MHz, yielding high damping rates. In order to minimize losses, high frequency interfacial Stoneley waves, which are nearly lossless by nature, have also been implemented for submicron manipulation.¹³

Regardless of their type, the application of BAW and SAW technologies to Lab-on-Chip science has become widespread across different fields, encompassing diverse specialities ranging from chemistry^{14,15} and chemical engineering¹⁶ to

^a Univ. Grenoble Alpes, F-38000 Grenoble, France

^b CEA LETI MINATEC Campus, F-38054 Grenoble, France.

E-mail: cedric.poulain@cea.fr; Tel: +33 04 3878 1508

^c Sorbonne Universités, UPMC Univ Paris 06, CNRS, UMR 7190, Institut Jean Le Rond d'Alembert, F-75005 Paris, France

^d Univ. Grenoble Alpes, IBS, F-38044 Grenoble, France

^e CNRS, IBS, F-38044 Grenoble, France

^f CEA, IBS, F-38044 Grenoble, France

† Electronic supplementary information (ESI) available. See DOI: 10.1039/c6lc00534a

biotechnologies.¹⁷ Despite the clear potential for commercial applications of acoustofluidic chips, their use in industry has so far remained limited essentially due to the cost and complexity of their fabrication in clean room conditions. Generic acoustic tweezers⁹ are currently made of materials such as silicon, glass or LiNbO₃ piezoelectric crystals, which are challenging to implement with existing fast-prototyping methods such as soft lithography and are relatively high-cost, low-reusability materials. It is particularly limiting for point of care applications for which a device has to be simple, reliable, low-cost, disposable, and portable.¹⁸ Recently, interesting approaches have been made to circumvent some of these limitations but both still require the use of a piezoelectric substrate or superstrate.^{11,18,19}

Here, we report a new strategy to achieve acoustic micro-manipulation, which relies on the use of subsonic surface waves leading to an evanescent acoustic field. As recently exploited in the context of acoustic streaming,²⁰ the use of an ultrathin substrate can slow down the surface wave velocity below the sound speed in the adjacent liquid leading to a subsonic regime. With a similar approach, we show that it is possible to excite a certain class of subsonic waves known as Scholte waves which are in essence quite different from the commonly used Rayleigh waves. Indeed, Rayleigh waves propagate in a supersonic regime, *i.e.* they travel faster in the substrate than in the adjacent liquid and consequently radiate sound into the fluid by emitting bulk waves at an angle θ (see Fig. 1a), so that they are highly damped while propagating along the substrate. This well-known feature explains why they are often referred as leaky Rayleigh waves.¹ On the contrary, Scholte waves are interfacial waves guided along a solid-liquid interface. They are always subsonic with respect to the speed of sound in the liquid and are consequently evanescent in the direction orthogonal to the interface.

Strictly speaking, Scholte waves refer solely to non dispersive waves which propagate along the interface between two semi-infinite solid and liquid media with a constant velocity smaller than the speed of sound in liquid. When the thickness of the solid plate is comparable with the Scholte wavelength, dispersion occurs and the wave is sometimes called a quasi-Scholte wave – see Cegla²¹ for a more detailed discussion. In other words, for a given finite substrate thickness,

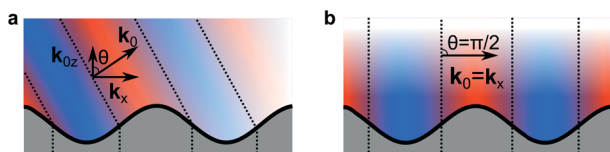


Fig. 1 (a) Supersonic regime of surface wave propagation: longitudinal waves are radiated away from the vibrating surface into the liquid at the Rayleigh angle $\theta = \sin^{-1}(c_0/c_x)$ where c_0 and c_x are respectively the liquid wave and substrate velocities. This radiation process leads to an attenuation of the wave along the substrate. (b) In the subsonic regime corresponding to $c_x < c_0$, the acoustic field of the surface wave is evanescent in the direction orthogonal to the surface. Consequently, the surface wave is not attenuated by radiation along the substrate.

the Scholte regime is a limit case which can be reached only at infinite frequency. The quasi-Scholte regime corresponds to the dispersive regime, which features a frequency dependent wave celerity often plotted as a function of the frequency \times thickness product. Here, we work in the dispersive (quasi-Scholte) regime, but for the sake of concision and since it is sometimes the case in the literature,²² we will often refer to the quasi-Scholte waves simply as Scholte waves.

The existence of Scholte waves has been first predicted in 1947 (ref. 23) as another type of solution of the dynamic equations of surface waves when loaded with a fluid. They have been experimentally evidenced first by de Billy *et al.*²⁴ followed by other works,^{25–27} and more recently used in the context of liquid sensing.^{21,28} So far, they have never been implemented for microfluidic applications, although they can be regarded as very promising for at least three reasons. Firstly, their propagation is lossless in the ideal case of absence of viscous or thermal dissipation. Hence, they can be generated far from the sample. Secondly, their propagation does not require any particular material. Thirdly, they are evanescent in the liquid, thus concentrating acoustic energy in the vicinity of the substrate where the particles are located and avoiding acoustic energy loss by radiation into the liquid bulk.

After a brief theoretical description of the properties of Scholte waves propagating along loaded plates, we describe a simple setup which enables to take advantage of this kind of waves for acoustofluidics applications. By means of both acoustic pressure measurements and schlieren imaging performed in a wide frequency range (0.2–3 MHz), we demonstrate their quasi-Scholte nature by measuring their velocity and comparing it to the theoretical dispersion equation as well as by revealing their evanescent nature in the liquid. Then, we illustrate different examples of key Lab-on-Chip applications obtained with a very simple device manufactured with common materials and without any need for clean room conditions. In particular, we show that standing quasi-Scholte waves emitted at a 0.5 W typical power are capable to arrange microbeads and living cells into regular arrays, to form plasma-enriched regions in whole blood and to rotate cells. Finally, we demonstrate their efficiency for concentrating microparticles flowing in a straight microchannel simply made up of tape.

Theoretical description of Scholte waves

The aim of this section is to theoretically describe the guided waves propagating along a plate. For that, we consider a homogeneous, isotropic, elastic plate with thickness d delimited by surfaces $z = \pm d/2$. The material constituting the plate is characterised by longitudinal and transverse bulk wave speeds c_L and c_T and density ρ . We assume the propagation of harmonic guided waves along the (Ox) axis with pulsation $\omega = 2\pi f$ and wavenumber k_x . Since the plate is assumed to be isotropic, guided waves being a linear combination of longitudinal and shear vertical waves propagate along the substrate independently of shear horizontal waves.

Assuming the plate to be surrounded by vacuum, the stress-free boundary conditions on both sides of the plate lead to two distinct dispersion equations for guided waves (see ESI† for details):

$$D_S = 4k_x^2 k_{Lz} k_{Tz} \tan\left(\frac{k_{Lz}d}{2}\right) + (k_{Tz}^2 - k_x^2)^2 \tan\left(\frac{k_{Tz}d}{2}\right) = 0, \quad (1)$$

$$D_A = 4k_x^2 k_{Lz} k_{Tz} \tan\left(\frac{k_{Lz}d}{2}\right) + (k_{Tz}^2 - k_x^2)^2 \tan\left(\frac{k_{Tz}d}{2}\right) = 0, \quad (2)$$

with $k_{Lz}^2 = k_L^2 - k_x^2$, $k_{Tz}^2 = k_T^2 - k_x^2$, $k_L = \omega/c_L$ and $k_T = \omega/c_T$. Eqn (1) (respectively 2) is the dispersion equation of the set of Lamb waves S_i (respectively A_i) (i being positive integer) characterised by a displacement field symmetric (respectively antisymmetric) with respect to the plate mid-plane. Now assuming the plate to be loaded on one side by a semi-infinite, inviscid liquid with mass density ρ_0 and sound speed c_0 , as sketched in the inset of Fig. 2, the dispersion equation can be concisely written as

$$D_S D_A = \frac{\rho_0 k_T^4 k_{Lz}}{\rho 2jk_{0z}} \left[\tan\left(\frac{k_{Lz}d}{2}\right) \tan\left(\frac{k_{Tz}d}{2}\right) D_A - D_S \right] \quad (3)$$

with $k_{0z}^2 = k_0^2 - k_x^2$, $k_0 = \omega/c_0$. Numerical resolution of eqn (3) in the particular case of interest for this study, *i.e.* a 150 μm thick glass‡ plate loaded with liquid water on one side, reveals three sets of waves: (i) two sets of modes, labelled S_i^* and A_i^* , which identify respectively with the S_i and A_i sets of Lamb waves in the $\rho_0/\rho \rightarrow 0$ limit, and called Lamb waves in the following, (ii) a quasi-Scholte mode which identifies in

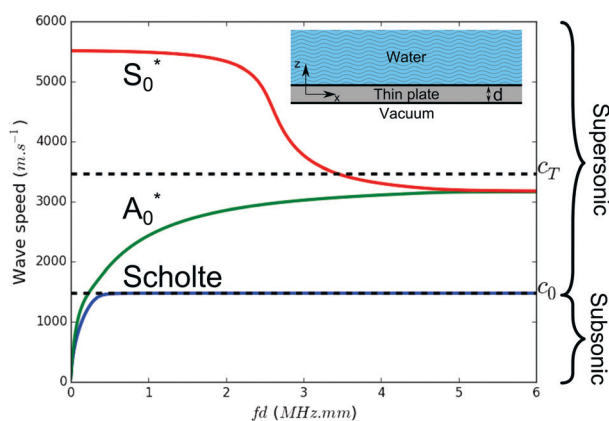


Fig. 2 Variation versus fd of the velocity of antisymmetric A_0^* and symmetric S_0^* Lamb waves and of Scholte wave propagating along a $d = 150 \mu\text{m}$ thick glass plate loaded on one side with an infinitely thick layer of water characterised by sound speed c_0 (see sketch in inset).

‡ The material is a D263 borosilicate glass characterized by $\rho = 2510 \text{ kg s}^{-3}$, $c_L = 5710 \text{ m s}^{-1}$, $c_T = 3470 \text{ m s}^{-1}$; pure water at room temperature is characterized by $\rho_0 = 1000 \text{ kg s}^{-3}$, $c_0 = 1480 \text{ m s}^{-1}$.

the $k_x d \rightarrow \infty$ limit with a Scholte wave and is called hereafter Scholte for all $k_x d$. We now focus our study on the slowest modes $i = 0$, which are generally the only modes used in actuation applications. As shown in Fig. 2, which displays the variations of the wave speed $\omega/\text{Re}(k_x)$ of the Lamb and Scholte waves versus the product fd , (i) the S_0^* Lamb wave is supersonic with respect to c_0 for all values of fd , (ii) the A_0^* Lamb wave is also supersonic except for $fd \leq 0.23 \text{ MHz mm}$, and (iii) the Scholte wave is always subsonic. These are the reasons why S_0^* and A_0^* Lamb waves radiate acoustic waves and are attenuated along their path on the plate while the Scholte waves are not (for an inviscid fluid). Accordingly, as shown in Fig. 3, which displays the variations of the amplitude attenuation per wavelength $\alpha_\lambda = 2\pi\text{Im}(k_x)/\text{Re}(k_x)$ of the Lamb and Scholte waves versus fd , even under the assumption of inviscid liquid, both S_0^* and A_0^* Lamb waves are noticeably attenuated while the Scholte wave is never.

Correlatively, k_{0z}^2 is real and negative for the Scholte wave, which implies that k_{0z} is purely imaginary: the Scholte wave does not radiate into the liquid bulk and the corresponding acoustic field in the liquid is evanescent. As shown in the inset of Fig. 3, which displays the evolution of the characteristic penetration thickness of the evanescent acoustic field of the Scholte wave in a semi-infinite liquid $(jk_{0z})^{-1}$ versus f , the acoustic energy carried by the Scholte wave is actually confined to a thin layer of the order of a few hundreds of microns in the investigated frequency range.

Experimental evidence of Scholte waves

Experimental setup

The device used to emit Scholte waves consists in a 10 mm \times 5 mm \times 0.66 mm piezo-transducer (Noliac NCE51) simply

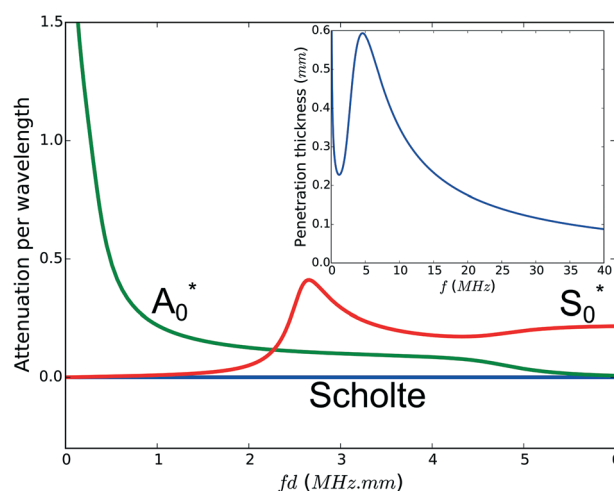


Fig. 3 Attenuation per wavelength as a function of fd of the antisymmetric A_0^* and symmetric S_0^* Lamb waves and of the Scholte wave propagating along a $d = 150 \mu\text{m}$ thick glass plate loaded on one side with an infinitely thick layer of water. Inset: Characteristic distance of penetration of the Scholte wave in the liquid $(jk_{0z})^{-1}$ as function of frequency.

glued onto the bottom side of a 60 mm × 24 mm × 150 μm glass plate (see Fig. 4). A channel consisting in two separated chambers and made from a special tape (Nitto Denko D53815) is glued onto the upper face of the thin glass plate. The cavity which does not face the piezo-transducer is filled with a 150 μm thick layer of pure water. The transducer is excited in sine mode at frequencies ranging from 200 kHz to 3 MHz by a function generator coupled with an AR 75A250A power amplifier.

We now demonstrate the Scholte nature of the plate waves generated using this device through (i) the measurement of their dispersion equation, (ii) the experimental evidence of their evanescent nature in the liquid, (iii) the identification of their conditions of reflection.

Assessment of the dispersion equation of Scholte waves

Since the generated plate waves are standing, the measurement of their dispersion equation is performed by measuring the distance between pressure nodes (or antinodes) as a function of frequency. Two complementary techniques have been implemented: acoustic pressure measurements and tracers.

At low frequencies (typ. below 500 kHz), the wavelength λ of the standing wave is assessed from acoustic pressure scans performed using a needle hydrophone (with 1 mm sensitive element diameter from Precision Acoustic) mounted on a translation plate actuated by a step micromotor (Newport NSA12). When moving steadily the microphone along the direction of propagation, the acoustic signal is recorded using a digital oscilloscope (Tektronix DPO 4032). The evolution of the pressure oscillation amplitude with position along the direction of propagation is displayed in Fig. 6a for $f = 312$ kHz. Assuming the distance between two extrema to be equal to a half-wavelength, λ is can be directly deduced.

At higher frequencies, the oscilloscope memory is not large enough and beads patterning is used instead. 40 μm diameter polymer beads (Duke Scientific 4240A series nanospheres) with density larger than unity, dispersed in water, are employed. When surface waves are generated on the chip, the beads arrange periodically into parallel rows after a transient of typically 10 s duration, as shown in Fig. 6b. The pitch of the beads pattern is equal to $\lambda/2$ as a consequence of the $\lambda/2$ spatial periodicity of the distribution of nonlinear acoustic forces.

The evolution of the surface wave speed $c_x = \lambda f$ deduced from these wavelength measurements as function of fd is

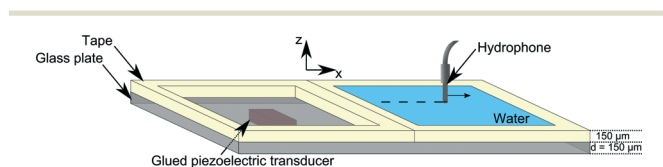


Fig. 4 Sketch of the experimental setup. The device is made of a piezo-transducer glued on the bottom side of a thin glass plate ($d = 150$ μm). On the opposite side, tape is used to form two cavities. The cavity which is not facing the transducer is filled with pure water. The hydrophone and its scanning direction are also shown.

displayed in Fig. 5 together with the theoretical dispersion curves for both the Scholte mode and Lamb mode A_0^* of a plate loaded on one side computed using eqn (3). Quantitative agreement between the dispersion curve of the Scholte wave and measurements is observed, which demonstrates that the acoustic field measured in water is associated to Scholte waves and not to loaded Lamb waves.

Evanescence of Scholte waves

As explained in the theoretical section, Scholte waves are evanescent in the direction orthogonal to the surface. In order to experimentally evidence the evanescent nature of the standing surface wave set up in the device, the chip is immersed in a transparent quartz container filled with water and care is taken to keep the transducer dry above the liquid surface. Schlieren imaging of the refractive index perturbations caused by the acoustic waves is implemented in order to visualise the pressure field in the vicinity of the glass plate. Details of the optical setup can be found in ESI.† A noticeable difference can be observed in the region close to the surface of the immersed plate when turning the sound on. The periodic light intensity pattern appearing close to the plate, see Fig. 7, renders the confinement of density perturbations in the liquid, as expected from the evanescent character of the wave.

Despite the fact that the plate is immersed, *i.e.* loaded on both sides, we have checked that this standing wave is actually a Scholte wave. The dispersion equation of antisymmetric elastic waves propagating along a plate loaded with an infinitely thick layer of water on both faces can be indeed written as:²⁹

$$D_A + j \frac{\rho_0}{\rho} \frac{k_T^4 k_{Lz}}{k_{0z}} = 0. \quad (4)$$

Numerical resolution of eqn (4) leads to a set of antisymmetric Lamb waves and a Scholte wave. The evolution *versus* fd of the Scholte wave speed computed using (4) is displayed in Fig. 5. The light intensity pattern being proportional to the acoustic intensity,³⁰ the spatial period of the schlieren pattern is equal to a half-wavelength. As shown in Fig. 5, quantitative agreement between the wave speed deduced from wavelength measurements and theory is observed, which demonstrates that in the case of a plate loaded on both sides the acoustic field measured in water is also associated to Scholte waves and not to Lamb waves.

Identification of the conditions of reflection of Scholte waves

The way the surface wave reflects at boundaries is also an indication of its structure. To investigate this, a 150 μm thick glass plate on which a transducer is glued is partially wetted with a 150 μm thick microbeads-loaded water layer along its transducer-free face, then covered by a similar glass plate, as sketched in Fig. 8a, in such a way that the air–water meniscus is not pinned on any glass edge. As shown in Fig. 8b and c, whatever the meniscus shape, close to the meniscus the periodic beads pattern formed by the standing

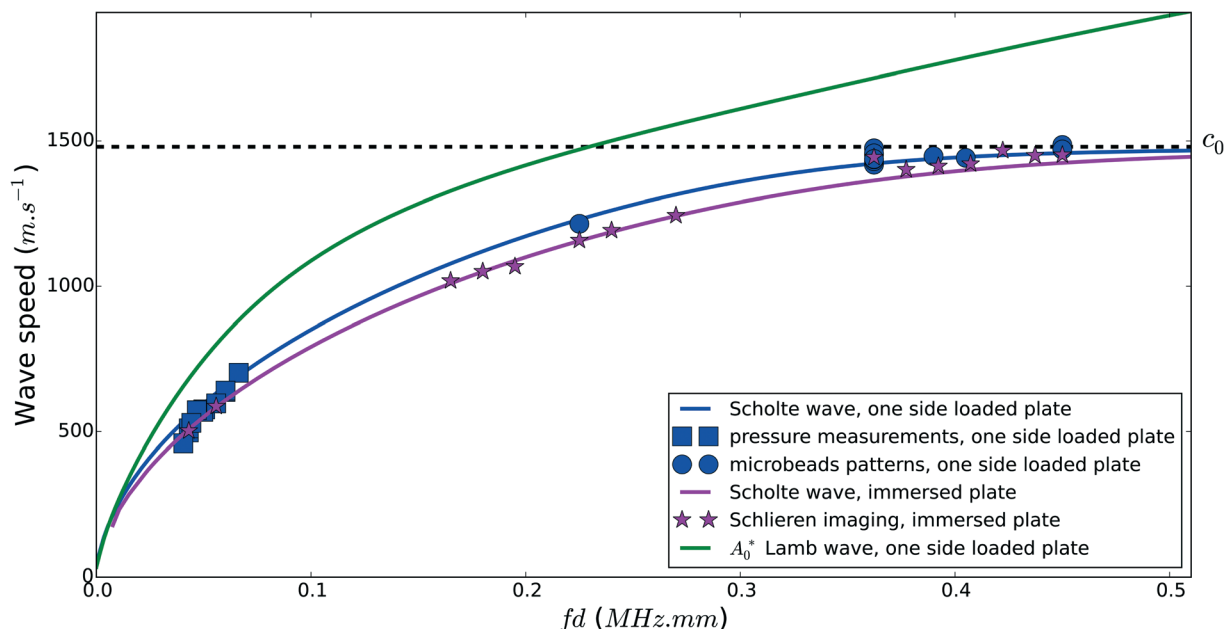


Fig. 5 Theoretical predictions (solid lines) of the fd -dependent velocity of A_0^* Lamb and Scholte waves are compared to the experimental determination of wave velocity from wavelength measurements (symbols) in order to identify the nature of the standing surface wave set up along plates loaded on one or both sides with water. Quantitative agreement between measurements and the predicted Scholte velocity in both cases demonstrate the Scholte nature of the surface wave obtained experimentally.

surface wave is parallel to the meniscus and not to the glass edge. This indicates that the surface wave responsible for the periodic arrangement of the beads is reflected by the meniscus and not by the glass edge. Moreover, by cutting the glass plate away from the meniscus, we have also checked that no modification of the patterns occurs regardless of the cutting angle. In other words, the acoustic cavity for the Scholte waves is determined by the liquid–solid region solely.

All these conclusions lead us to claim that the standing surface waves set up along a thin, liquid-loaded glass plate by a longitudinal piezoelectric transducer simply glued on the

plate is essentially a Scholte wave, which has a subsonic speed and confines acoustic energy close to the plate. We now demonstrate that such a simple and low-cost device can be used for achieving several key-operations in microfluidics.

Microfluidic applications of Scholte waves

Regular arrangement and concentration of cells under flow

Here we show that standing Scholte waves can be used to pattern and concentrate flowing cell suspensions in microchannels. The device consists in a $150\ \mu\text{m} \times 1.5\ \text{mm}$ rectangular microchannel formed between a $150\ \mu\text{m}$ thick glass plate and a $1\ \text{mm}$ thick PMMA plate parallel to each other. Channel walls are simply made of $150\ \mu\text{m}$ thick tape (see Fig. 9). A suspension of HeLa cells fixed in a paraformaldehyde 2% solution is injected into the microchannel at a $7\ \mu\text{L}\ \text{min}^{-1}$ flow rate through holes in the PMMA plate. The piezotransducer is glued parallel to the channel on the outer face of the glass plate. When the power supply is off, the suspension flows homogeneously along the channel, as shown in Fig. 9a. When a $f = 2.515\ \text{MHz}$ sine signal is applied to the transducer, the flowing suspension organises into straight stripes characterised alternatively by a high/low cell concentration with a $\lambda/2$ spacing, as shown in Fig. 9c. This example illustrates the ease of implementation of Scholte waves in microchannels.

Single cell trapping and rotation

Acoustic forces are well-known as a powerful tool to arrange particles or living cells in a contact-less manner. Exerting a

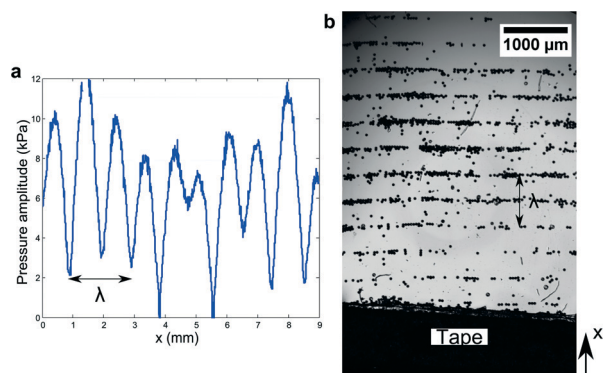


Fig. 6 Measurement of the wavelength of the standing surface wave obtained using the setup sketched in Fig. 4. (a) A needle hydrophone has been used to measure the pressure oscillation amplitude as function of position along the propagation axis of the surface wave. Acoustic frequency is $f = 312\ \text{kHz}$. (b) $40\ \mu\text{m}$ diameter polymer beads align along pressure nodes of a $f = 1.5\ \text{MHz}$ standing surface wave. See video in ESI.†

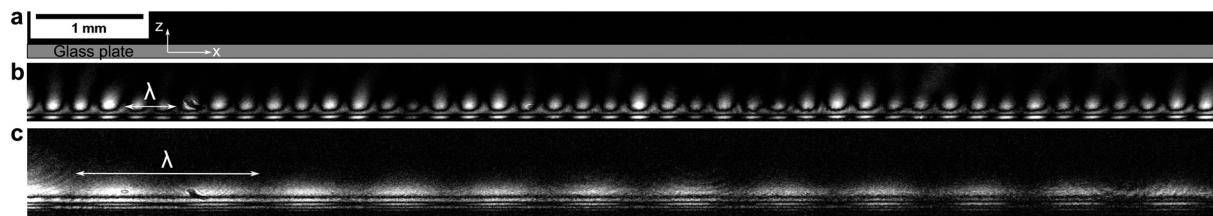


Fig. 7 Evidence of the evanescent nature of the acoustic field of the standing Scholte wave in water from sideways schlieren imaging of a 150 μm thick glass plate immersed in pure water (a) without acoustic excitation, (b) with acoustic excitation at frequency $f = 2715$ kHz and (c) $f = 287$ kHz.

mechanical torque at microscale on a microparticle is also possible although it requires a more complex pressure field composed of two independent waves of same frequency. Indeed, since the pioneering work of Busse,³¹ it is known that when a scatterer immersed in a fluid is submitted to an acoustic standing field resulting from the superposition of two plane, perpendicular, harmonic standing waves with a $\pi/2$ phase shift, the combination of nonlinear and dissipative phenomena in the viscous boundary layer around the scatterer results in a viscous torque exerted on the scatterer, which depends on the scatterer location. The map of the two-dimensional, λ -periodic torque distribution associated to such an acoustic field is shown in Fig. 10b. It exhibits alternate clockwise and anticlockwise areas. Such a torque field can be used to steadily rotate particles trapped in nodes of the standing acoustic field.³² In order to implement this specific actuation for individual cells, two piezo-transducer are glued perpendicular to each other on a 150 μm thick glass plate, see Fig. 10a. This vibrating plate covers a drop of dilute suspension of fixed HeLa cells deposited on a 1 mm thick glass plate. Both piezo-transducers are excited by a two output function generator (Tektronix AFG 3102C) on which the phase lag and amplitude are set such that after independent

amplification, amplitudes are equal and the phase shift is exactly equal to $\pi/2$. When the sound is turned on, HeLa cells migrate towards pressures nodes and start spinning at a typical rotation rate of 0.25 cycle per second, see Fig. 10c. As expected, cells rotate in clockwise and anticlockwise directions according to the predicted torque field. This periodic arrangement in the form of an array together with the associated alternated rotation might open the route towards an automated screening of some mechanical features of living cells (state, size, elasticity,...) for a given cell population and type.

Periodical arrangement of diluted RBC and local depletion in whole blood

Whole blood manipulation is also crucial for point of care applications where blood taken from a patient has to be examined and characterised. Here, we show that Scholte waves are powerful enough to handle a drop of whole blood of volume as small as 30 μL . Taking advantage of the previously presented device developed for acoustorotation, we observe that an initially opaque drop can be made non homogeneous thanks to the acoustic forces within typically ~ 10 s. It leads to the appearance of bright zones which are cells depleted and hence plasma enriched, surrounded by dark regions where most cells migrate and concentrate, as shown in Fig. 11b. This patterning within the blood drop in a very simple device is also promising for disposable and portable applications when the blood has to be featured. Indeed, most compounds in the whole blood (glycemia, cholesterol, creatinine *etc.*)

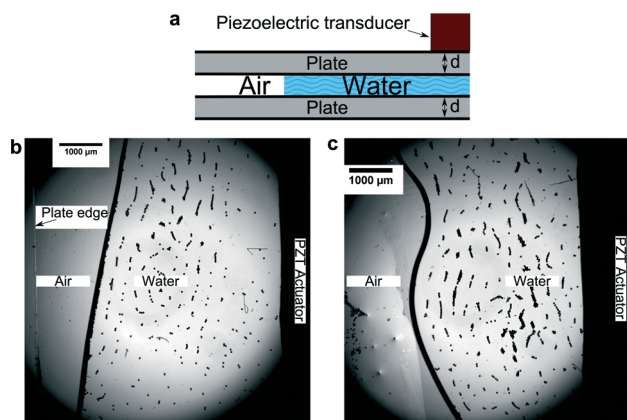


Fig. 8 In order to determine how the air-water interface influences the propagation of the Scholte wave, a suspension of 40 μm diameter polymer beads partially fills the cavity of the setup sketched in Fig. 4 and is covered by a glass plate. (a) Sideways sketch of the experimental setup. (b) and (c) Top views of the suspension submitted to acoustic excitation at $f = 2575$ kHz. Close to the meniscus, the steady beads pattern is parallel to the meniscus whatever the shape of the meniscus and of the glass plate. This indicates that Scholte waves are actually reflected by the meniscus.

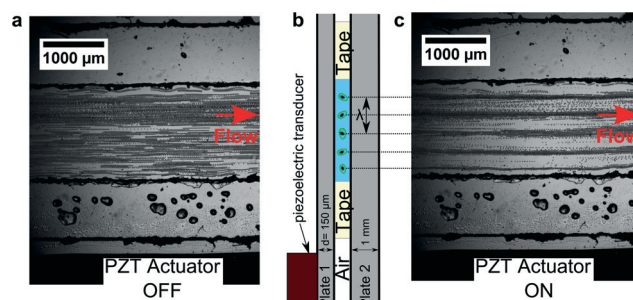


Fig. 9 Tape-made microfluidic channel sandwiched between a thin glass plate excited by a piezo-transducer and a PMMA cover plate. Two holes are made in the PMMA in order to allow tubing and fluid supply. A water solution of fixed HeLa cells flows through the microchannel. (a) In the absence of sound, cells are homogeneously distributed within the microchannel. (b) Sideways sketch of the experimental setup. (c) When turning the sound on, flowing HeLa cells concentrate along parallel lines in the flow.

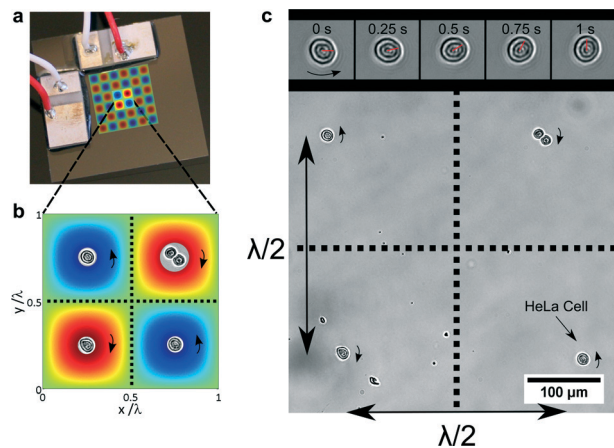


Fig. 10 (a) Acoustorotation chip made of two transducers glued on a glass plate used to obtain cell trapping and rotation. (b) Two-dimensional, λ -periodic acoustic torque distribution in a one wavelength square element. The clockwise rotation triggered by the acoustic torque is represented in red colour while anticlockwise rotating in blue. The green colour indicates zero torque amplitude. (c) Picture of HeLa cells trapped in the four traps lying in a one wavelength long square when submitted to an acoustic field of frequency $f = 2415$ kHz in agreement with the theoretical prediction. Top: Successive snapshots of a single rotating HeLa cell. See video in ESI†

are actually measured within the plasma and could easily be optically measured through the bright zones of the enriched plasma regions in a simple blood droplet. Diluting blood and exciting only one piezo-transducer, we recover the periodic linear pattern reported above, see Fig. 11a.

Discussion

We have shown that Scholte waves can be generated along a thin glass plate and used in microfluidics for Lab-on-Chip applications. By combining acoustic pressure measurements, patterning of microparticles driven by acoustic forces and schlieren imaging, we have undoubtedly demonstrated that ultrasonic plate waves are mainly Scholte waves, *i.e.* subsonic waves with respect to the speed of sound in water, and not leaky Lamb waves. Their subsonic nature results in an evanescent acoustic field perpendicular to the plate surface.

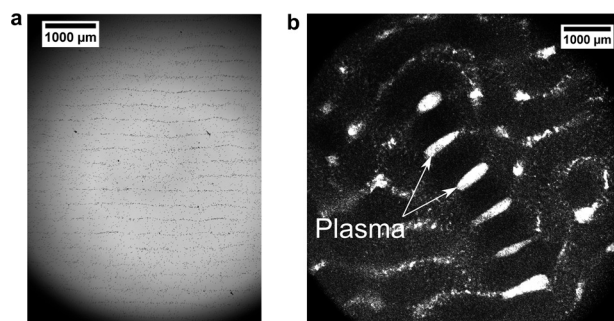


Fig. 11 (a) Periodical arrangement of red blood cells of diluted whole blood under 1D acoustic excitation at $f = 2415$ kHz. (b) Depletion zones (pure plasma) appearing in whole blood when the sample is submitted to a 2D acoustic field tuned for acoustorotation. See video in ESI†

The evanescent nature of the acoustic field of the Scholte wave in the liquid appears as an ideal asset in the context of microfluidics. Indeed, since acoustic energy is confined close to the plate and does not radiate into the liquid bulk, this allows for efficient acousto-actuation close to the substrate with a minimal energy. As shown in Cegla *et al.*²¹ in the case of an aluminium plate in a comparable frequency-thickness range, a noticeable amount of energy (at least half) is carried by the Scholte wave through the liquid.

In the reported experiments, the electric power consumption has been estimated to be of the order of 0.5 W (see ESI†), which leads to typically 10–100 kPa in the corresponding frequency range 300 kHz–3 MHz, in agreement with pressure measurements obtained with the hydrophone. § These values show that efficient and low consumption evanescent actuation is possible even at relatively low frequency. As noted in the introduction, acoustic radiation forces scale as the spatial gradient ($\sim \lambda^{-1}$) of the Gor'kov potential. We point out that the strong dispersion of quasi-Scholte waves (see Fig. 2) results in wavelengths smaller than those of non dispersive Bulk or Rayleigh waves along thick substrates in the low frequency region. Therefore, taking advantage of the strong dispersive character of thin plate waves at low frequency is an interesting strategy for acoustic actuation.

Conclusion

In this paper, we have reported several examples of key-applications in acoustofluidics using Scholte waves by taking advantage of a very simple and low-cost device. We have shown that a very thin plate on which a piezo-transducer is glued consists in a very simple Scholte wave emitter capable to exert strong and well defined force or torque fields upon microparticles or cells. The evanescence of the field in the direction orthogonal to the plate confines the acoustic energy close to the channel walls where the particles to be moved are located instead of radiating it into the whole bulk fluid or through the chip. In particular, we have shown how to use this device for efficiently forming lines or arrays of living cells in a few seconds which could simplify Lab-on-Chip 3D cell printing for tissue engineering applications or cell identification.

We have also demonstrated single cell acoustorotation of individual cells in an array by superimposing two orthogonal out of phase Scholte waves. Although acoustorotation is beyond the scope of this particular study, we believe that acoustorotation by Scholte waves could open the route to 3D cell scanning tomography or cell featuring by instantaneously screening a whole cell population. Finally, using whole blood,

§ We have also confirmed this order of magnitude by an indirect force measurement assuming that the classic Gor'kov model still applies in an evanescent field: by tracking the beads velocity using Trackmate from ImageJ and by integrating their trajectory to get to the force field (using a classic procedure as described in ref. 10) we have inferred an acoustic energy density of the order of 1 J m^{-3} and equivalently an acoustic pressure around 100 kPa at 3 MHz.

we have shown how to create plasma enriched regions in a drop sandwiched between two parallel plates with a 150 μm gap. Again, it is noteworthy that these chips can be manufactured out of clean room, by simply using tape as channel walls and a commercial glass cover slide for propagating Scholte waves. We hope this approach will stimulate new point of care applications for which a low-cost manufacturing remained an obstacle.

Acknowledgements

This work has been partly funded by the Technologie pour la Sante program of the CEA. The authors thank F. Lacroix for the access to the Cell Imaging Facility of the Grenoble Instruct Centre (ISBG; UMS 3518 CNRS-CEA-UJF-EMBL) supported by FRISBI (ANR-10-INSB-05-02) and GRAL (ANR-10-LABX-49-01). The authors also thank Antoine Delon for his help in electrical measurements.

References

- J. Friend and L. Y. Yeo, *Rev. Mod. Phys.*, 2011, **83**, 647–704.
- H. Bruus, *Lab Chip*, 2011, **11**, 3742–3751.
- B. Raeymaekers, C. Pantea and D. N. Sinha, *J. Appl. Phys.*, 2011, **109**, 014317.
- D. Rabaud, P. Thibault, J.-P. Raven, O. Hugon, E. Lacot and P. Marmottant, *Phys. Fluids*, 2011, **23**, 042003.
- A. Hashmi, G. Yu, M. Reilly-Collette, G. Heiman and J. Xu, *Lab Chip*, 2012, **12**, 4216–4227.
- D. J. Collins, B. Morahan, J. Garcia-Bustos, C. Doerig, M. Plebanski and A. Neild, *Nat. Commun.*, 2015, **6**, 8686.
- J. D. N. Cheeke, *Fundamentals and applications of ultrasonic waves*, CRC press, 2012.
- R. Barnkob, P. Augustsson, T. Laurell and H. Bruus, *Lab Chip*, 2010, **10**, 563–570.
- S. B. Q. Tran, P. Marmottant and P. Thibault, *Appl. Phys. Lett.*, 2012, **101**, 114103, mult. p.
- H. Bruus, *Lab Chip*, 2012, **12**, 1014–1021.
- A. R. Rezk, J. R. Friend and L. Y. Yeo, *Lab Chip*, 2014, **14**, 1802–1805.
- A. Haake and J. Dual, *Ultrasonics*, 2004, **42**, 75–80.
- V. Yantchev, J. Enlund, I. Katardjiev and L. Johansson, *J. Micromech. Microeng.*, 2010, **20**, 035031.
- T. Laurell, F. Petersson and A. Nilsson, *Chem. Soc. Rev.*, 2007, **36**, 492–506.
- P.-H. Huang, C. Y. Chan, P. Li, N. Nama, Y. Xie, C.-H. Wei, Y. Chen, D. Ahmed and T. J. Huang, *Lab Chip*, 2015, **15**, 4166–4176.
- Y. Xie, C. Chindam, N. Nama, S. Yang, M. Lu, Y. Zhao, J. D. Mai, F. Costanzo and T. J. Huang, *Sci. Rep.*, 2015, **5**, 12572.
- M. Antfolk, C. Antfolk, H. Lilja, T. Laurell and P. Augustsson, *Lab Chip*, 2015, **15**, 2102–2109.
- F. Guo, Y. Xie, S. Li, J. Lata, L. Ren, Z. Mao, B. Ren, M. Wu, A. Ozcelik and T. J. Huang, *Lab Chip*, 2015, **15**, 4517–4523.
- H. Jin, J. Zhou, X. He, W. Wang, H. Guo, S. Dong, D. Wang, Y. Xu, J. Geng and J. Luo, *et al.*, *Sci. Rep.*, 2013, **3**, 2140.
- G. Vuillermet, P.-Y. Gires, F. Casset and C. Poulain, *Phys. Rev. Lett.*, 2016, **116**, 184501.
- F. Cegla, P. Cawley and M. Lowe, *J. Acoust. Soc. Am.*, 2005, **117**, 1098–1107.
- J. L. Rose, *Ultrasonic guided waves in solid media*, Cambridge University Press, 2014.
- J. G. Scholte, The Range of Existence of Rayleigh and Stoneley Waves, *Geophys. J.*, 1947, **5**, 120–126.
- M. de Billy and G. Quentin, *J. Appl. Phys.*, 1983, **54**, 4314–4322.
- F. Luppé and J. Doucet, *J. Acoust. Soc. Am.*, 1988, **83**, 1276–1279.
- C. Glorieux, K. Van de Rostyne, K. Nelson, W. Gao, W. Lauriks and J. Thoen, *J. Acoust. Soc. Am.*, 2001, **110**, 1299–1306.
- J. Zhu, J. S. Popovics and F. Schubert, *J. Acoust. Soc. Am.*, 2004, **116**, 2101–2110.
- A. Takiy, S. Granja, R. Higuti, C. Kitano, L. Elvira, O. Martinez-Graullera and F. Montero de Espinosa, *et al.*, 2013 *Ieee International Ultrasonics Symposium (ius)*, 2013, pp. 1610–1613.
- I. A. Viktorov, *Rayleigh and Lamb waves: physical theory and applications*, Plenum press, 1970.
- G. S. Settles, in *Schlieren and Shadowgraph Techniques: Visualizing Phenomena in Transparent Media*, Springer Berlin Heidelberg, Berlin, Heidelberg, 2001, ch. Socialized Schlieren Techniques, pp. 111–141.
- F. Busse and T. Wang, *J. Acoust. Soc. Am.*, 1981, **69**, 1634–1638.
- A. Lamprecht, T. Schwarz, J. Wang and J. Dual, *J. Acoust. Soc. Am.*, 2015, **138**, 23–32.